



# Transport of ARS-labeled hydroxyapatite nanoparticles in saturated granular media is influenced by surface charge variability even in the presence of humic acid

Dengjun Wang<sup>a,d</sup>, Scott A. Bradford<sup>b</sup>, Ronald W. Harvey<sup>c</sup>, Xiuzhen Hao<sup>a</sup>, Dongmei Zhou<sup>a,\*</sup>

<sup>a</sup> Key Laboratory of Soil Environment and Pollution Remediation, Institute of Soil Science, Chinese Academy of Sciences, No. 71 East Beijing Road, Nanjing 210008, China

<sup>b</sup> U.S. Salinity Laboratory, Agricultural Research Service, United States Department of Agriculture, 450 W. Big Springs Road, Riverside, CA 92507, United States

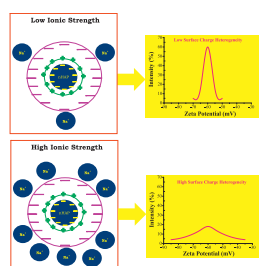
<sup>c</sup> U.S. Geological Survey, 3215 Marine Street, Boulder, CO 80303, United States

<sup>d</sup> Graduate School of the Chinese Academy of Sciences, Beijing 100049, China

## HIGHLIGHTS

- ▶ The transport and retention kinetics of ARS-labeled hydroxyapatite nanoparticles (ARS-nHAP) were investigated over a range of ionic strengths in the presence of humic acid.
- ▶ A two-site kinetic attachment model predicted both the breakthrough curves and retention profiles of ARS-nHAP quite well.
- ▶ The retention profiles of ARS-nHAP exhibited hyperexponential shapes for all the test conditions.
- ▶ Surface charge heterogeneities on the collector surfaces and especially within the ARS-nHAP population contributed to hyperexponential retention profiles.

## GRAPHICAL ABSTRACT



## ARTICLE INFO

### Article history:

Received 24 February 2012

Received in revised form 18 May 2012

Accepted 25 May 2012

Available online 2 June 2012

### Keywords:

ARS-labeled hydroxyapatite nanoparticles

(ARS-nHAP)

Ionic strength ( $I_c$ )

Breakthrough curve (BTC)

Retention profile (RP)

Colloid filtration theory (CFT)

## ABSTRACT

Hydroxyapatite nanoparticle (nHAP) is increasingly being used to remediate soils and water polluted by metals and radionuclides. The transport and retention of Alizarin red S (ARS)-labeled nHAP were investigated in water-saturated granular media. Experiments were carried out over a range of ionic strength ( $I_c$ , 0–50 mM NaCl) conditions in the presence of 10 mg L<sup>-1</sup> humic acid. The transport of ARS-nHAP was found to decrease with increasing suspension  $I_c$  in part, because of enhanced aggregation and chemical heterogeneity. The retention profiles (RPs) of ARS-nHAP exhibited hyperexponential shapes (a decreasing rate of retention with increasing transport distance) for all test conditions, suggesting that some of the attachment was occurring under unfavorable conditions. Surface charge heterogeneities on the collector surfaces and especially within the ARS-nHAP population were contributing causes for the hyperexponential RPs. Consideration of the effect(s) of  $I_c$  in the presence of HA is needed to improve the efficacy of nHAP for scavenging metals and actinides in real soils and groundwater environments.

© 2012 Elsevier B.V. All rights reserved.

## 1. Introduction

Hydroxyapatite nanoparticle (Ca<sub>10</sub>(PO<sub>4</sub>)<sub>6</sub>(OH)<sub>2</sub>, nHAP), due to its strong adsorptive properties for hazardous materials, is increas-

\* Corresponding author. Tel.: +86 25 86881180; fax: +86 25 86881000.  
E-mail address: [dmzhou@issas.ac.cn](mailto:dmzhou@issas.ac.cn) (D. Zhou).

ingly used in sequestration of metals and actinides in wastewater and nuclear waste disposal [1–4]. However, little attention has been paid to study the fate and transport of nHAP in granular environments. In order to track its transport and distribution in saturated granular media, nHAP was covalently bonded with the fluorescent label Alizarin red S (ARS) [5].

The role of ionic strength ( $I_c$ ) in enhancing the aggregation and deposition of colloids including nanoparticles (NPs) in granular media is well-documented [6]. Increases in solution  $I_c$  will decrease the thickness of the electrical double layer (EDL) and magnitude of the surface charge. Derjaguin–Landau–Verwey–Overbeek (DLVO) [7,8] theory predicts that NP aggregation and retention will increase with  $I_c$  due to a reduction in the height of the repulsive energy barrier and an increase in the depth of the secondary minimum. The influence of microscopic charge heterogeneities on NP retention is also expected to increase with  $I_c$  [9,10]. Natural organic matter (e.g., humic acid, HA) in soils and groundwater environments can partition onto NPs and thereby alter their transport behaviors [11–13]. Our previous study confirmed that even a minute amount of HA (e.g.,  $1 \text{ mg L}^{-1}$ ) can substantially enhance the transport of ARS-nHAP in saturated sand by masking charge heterogeneities that would otherwise decrease the propensity for aggregation and (or) attachment [5,14]. However, until now, there have been no systematic, quantitative investigations concerning the effect of  $I_c$  on the transport behavior of ARS-nHAP in the presence of HA.

Surface charge heterogeneities among colloidal particles and stationary grains in granular media have been shown to affect the magnitude of NP retention and to contribute to hyperexponential-shaped RPs [15–18]. One potential explanation for the preferential deposition of colloids closer to the column inlet is the distribution of interaction potentials among that colloid population [15]. Surface charge heterogeneity within the collector surfaces has also been demonstrated to produce “favorable nanoscale patches” for NP retention and the magnitude of the “favorable nanoscale patches” increased with  $I_c$  due to compression of the NPs EDL [9,10]. In a previous study [5], it was unclear whether surface charge heterogeneity was contributing to the observed hyperexponential RPs for ARS-nHAP. In particular, it was not known whether the surface charge heterogeneity within the ARS-nHAP population varied with  $I_c$  in the presence of environmental levels of HA, which could potentially mask surface charge heterogeneity [5,13].

The main objective of this study was to systemically investigate the coupled effects of solution  $I_c$  and HA on the transport and retention behavior of ARS-labeled nHAP in water-saturated, sand-packed columns. A secondary objective was to investigate the specific contributions to hyperexponential RPs caused by surface charge heterogeneities in ARS-nHAP and collector (sand grains).

## 2. Materials and methods

### 2.1. ARS-labeled nHAP

nHAP (purity >99%) was purchased from Aipurui Nanomaterial, Inc., Nanjing, China. Detailed characterization of nHAP was performed in our previous work [19]. Briefly, nHAP is 20 nm wide and 100 nm long. It has a Ca/P molar ratio of 1.65 and a specific surface area of  $154 \text{ m}^2 \text{ g}^{-1}$ , respectively. Alizarin red S (ARS,  $\text{C}_{14}\text{H}_7\text{NaO}_7\text{S}$ ) was successfully used as a label to facilitate tracking the movement of nHAP NPs through water-saturated, granular media. The ARS-labeled nHAP (ARS-nHAP) was prepared following the procedure reported elsewhere [20] and detailed information may be found in our previous work [5].

Stable aqueous ARS-nHAP suspensions were prepared by adding 20 mg of ARS-nHAP powder to 200 mL of  $10 \text{ mg L}^{-1}$  HA solution

(HA stock solution was introduced in the Supporting Information 1, S11) at desired  $I_c$  conditions (Table 1), stirring for 1 min, and sonicating (100 W, 45 kHz, KQ-300VDE sonicator, Shanghai, China) for 30 min at  $25^\circ\text{C}$  to ensure homogeneous suspensions. The resulting suspension obtained  $100 \text{ mg L}^{-1}$  ARS-nHAP.

### 2.2. Column transport experiments

Quartz sand obtained from Sinopharm Chemical Reagent Co., Ltd., China (26–30 mesh, 0.55–0.65 mm, 0.6 mm median grain size), was served as the granular media in the column tests. Prior to use, the sand was cleaned using a previously described procedure [21].

Transport tests were conducted in 2.6 cm diameter, 20.0 cm long glass chromatography columns fitted on both ends of the column with polytetrafluoroethylene end-caps and stainless-steel mesh (80  $\mu\text{m}$  openings). The columns were wet-packed using the procedure described in our previous study [21]. Porosity of the packed columns varied between 0.38 and 0.40.

Columns were run in an upflow mode using a peristaltic pump (Model YZII-15, Baoding Longer Precision Pump Co., Ltd., Hebei, China) and equilibrated by sequentially pumping  $\sim 10$  pore volumes (PVs) of deionized (DI) water (18.2 M  $\Omega$ , Millipore, Inc., USA) followed by at least 10 PVs of the ARS-nHAP-free background electrolyte solution (in the absence of HA) at desired  $I_c$  through the column at a constant Darcy velocity of  $7.5 \times 10^{-3} \text{ cm s}^{-1}$ . A stable ARS-nHAP suspension (see Table 1) with the same background electrolyte composition was then injected into the column for about 4 PVs, followed by several PVs of background electrolyte solution to ensure that the effluent was free of ARS-nHAP. Column effluent was collected using a fraction collector (Model BS-110A, Huxi Analytical Instrument Factory Co., Ltd., Shanghai, China). The concentrations of ARS-nHAP in the effluent were determined spectrophotometrically at wavelength of 518 nm [22] (Model 721-100, Jinghua Science and Technology Instrument Co., Ltd., Shanghai, China). A calibration curve was constructed by diluting the  $100 \text{ mg L}^{-1}$  ARS-nHAP suspension, which was linear within the range of 0–100  $\text{mg L}^{-1}$ . The lower detection limit was as low as  $0.2 \text{ mg L}^{-1}$ .

Following the completion of each transport test, each column was carefully dissected into 10 layers of 2 cm thick segments. The retained ARS-nHAP in each fraction was then recovered in the presence of DI water in order to determine the retention profiles, as described earlier [23,24]. A mass balance was calculated by comparing the quantity of ARS-nHAP in the effluent and retained in the sands to that injected into the column. All transport tests were performed at least in duplicate.

### 2.3. Electrokinetic properties of ARS-nHAP and sand grains

Electrophoretic mobilities were conducted using microelectrophoresis (Zhongcheng Digital Technology model JS94G, Shanghai, China) at  $25^\circ\text{C}$ , as described earlier [19,21], and converted to zeta potentials ( $\zeta$ ) using the Smoluchowski equation [25]. This  $\zeta$ -potential information was used in conjunction with DLVO theory to calculate the average interaction energy of ARS-nHAP with the sand grain (Supporting Information, S12).

### 2.4. ARS-nHAP size analysis

Suspensions of ARS-nHAP ( $100 \text{ mg L}^{-1}$ ) were air-dried on 400-mesh, carbon-coated Cu transmission electron microscopy (TEM) grids (Ted Pella, Redding, CA). The morphology, structure, and size of the ARS-nHAP were then measured using TEM (JEOL JEM-2100, Japan).

The average ARS-nHAP aggregate size and the intrinsic size distributions in various influent and select effluent suspensions were determined by dynamic light scattering (DLS) using a

**Table 1**  
Electrokinetic properties and mass balances for ARS-nHAP suspensions at varying ionic strengths ( $I_c$ ) used in transport tests.

$I_c^a$ (mM)	$\zeta_g^b$ (mV)	$\zeta_{\text{ARS-nHAP}}^b$ (mV)	$\Phi_{\text{max}}^c$ ( $K_B T$ )	$\Phi_{\text{min}2}^c$ ( $K_B T$ )	$h^d$ (nm)	$M_{\text{eff}}^e$ (%)	$M_{\text{ret}}^e$ (%)	$M_{\text{tot}}^e$ (%)
0.1	-63.2	-58.7	276	-0.075	318	78.8	24.9	104
1.0	-60.3	-48.5	203	-0.26	89	55.3	45.5	101
10	-37.1	-38.5	104	-0.87	22	41.7	58.4	100
50	-21.4	-27.7	37	-1.7	8	7.8	93.0	101

<sup>a</sup> The ARS-nHAP suspended in different concentrations of NaCl solutions (pH 7.2 and HA = 10 mg L<sup>-1</sup>).

<sup>b</sup> Refer to  $\zeta$ -potentials of quartz colloid and ARS-nHAP, respectively.

<sup>c</sup> Refer to maximum energy barrier and secondary minimum, respectively, calculated by DLVO theory.

<sup>d</sup> Separation distance from colloid surface to secondary minimum.

<sup>e</sup> Refer to the effluent, retained, and total percentages of ARS-nHAP from column experiments, respectively.

multi-detector light unit which employs a laser with a wavelength of 640 nm (Brookhaven Instruments model BI-200SM, Holtsville, NY). For each experiment, 3 mL of 100 mg L<sup>-1</sup> ARS-nHAP suspension was input into a glass vial which had been soaked in cleaning solution, thoroughly rinsed with DI water, and oven-dried under dust-free conditions. The scattered light intensity was detected by a photodetector at a scattering angle of 90°, and each auto-correction function was accumulated for 15 s. The intensity-weighted hydrodynamic particle size distributions were determined from the intensity-autocorrelation functions using the NNLS algorithm assuming the Stokes-Einstein equation [25]. The intensity-weighted particle size distributions were subsequently converted to number-weighted size distributions. The latter number-weighted sizes were used in the DLVO energy calculations. All characterization measurements were conducted in at least duplicate using freshly prepared suspensions for each condition.

### 2.5. Transport model

A one-dimensional form of the advection–dispersion equation with two-site kinetic retention was used to simulate the ARS-nHAP transport and retention [26,27]:

$$\frac{\partial \theta C}{\partial t} + \rho_b \frac{\partial (s_1)}{\partial t} + \rho_b \frac{\partial (s_2)}{\partial t} = \frac{\partial}{\partial x} \left( \theta D \frac{\partial C}{\partial x} \right) - \frac{\partial q C}{\partial x} \quad (1)$$

where  $\theta$  is the volumetric water content [–],  $C$  is the ARS-nHAP concentration in the aqueous concentration [N L<sup>-3</sup>, where  $N$  and  $L$  denote number and length, respectively],  $t$  is the time [T],  $\rho_b$  is the bulk density of the porous matrix [M·L<sup>-3</sup>, where  $M$  denotes mass],  $x$  is the vertical spatial coordinate [L],  $q$  is the Darcy velocity [L·T<sup>-1</sup>], and  $s_1$  [N·M<sup>-1</sup>] and  $s_2$  [N·M<sup>-1</sup>] are the solid phase concentrations associated with retention site types 1 and 2, respectively.

The two kinetic retention sites control mass transfer of ARS-nHAP between the aqueous and solid phase. The first kinetic site (site 1, Eq. (2)) assumes reversible (i.e., deposited in the secondary minimum), time-dependent retention, whereas the second kinetic site (site 2, Eq. (3)) assumes irreversible, depth-dependent retention as:

Site 1:

$$\rho_b \frac{\partial (s_1)}{\partial t} = \theta k_1 C - \rho_b k_{1d} s_1 \quad (2)$$

Site 2:

$$\rho_b \frac{\partial (s_2)}{\partial t} = \theta k_2 \psi_x C \quad (3)$$

where  $k_1$  [T<sup>-1</sup>] and  $k_2$  [T<sup>-1</sup>] are the first-order retention coefficients on sites 1 and 2, respectively,  $k_{1d}$  [T<sup>-1</sup>] is the first-order detachment coefficient, and  $\psi_x$  [–] is a dimensionless function to account for depth-dependent retention.

$$\psi_x = \left( \frac{d_c + x - x_0}{d_c} \right)^{-\beta} \quad (4)$$

where  $d_c$  is the median diameter of the sand grains [L] and  $\beta$  [–] is an empirical factor controlling the shape of the spatial distribution. Bradford et al. [26] found that a value of  $\beta = 0.432$  provides an optimum for experiments in which significant depth-dependency occurred and this value is assumed herein.

BTCs and RPs were analyzed using the HYDRUS-1D code [28] which solves Eqs. (1)–(4) numerically. A nonlinear least square optimization routine based on the Levenberg–Marquardt algorithm [29] is incorporated in the HYDRUS-1D code to fit the nHAP transport parameters ( $k_1$ ,  $k_{1d}$ , and  $k_2$ ). The outlined transport model is viewed as a simple and flexible approach to describe ARS-nHAP breakthrough curves and retention profiles that are not exponential with depth, with retention near the column inlet dominated by irreversible (site 2) retention and away from the inlet by reversible (site 1) retention. In this work, we did not attempt to attribute specific ARS-nHAP retention mechanisms to a given retention site without additional experimental evidence except for the retention of NPs in the secondary minimum (site 1) as mentioned above.

## 3. Results and discussion

### 3.1. Electrokinetic properties of ARS-nHAP and sand grain

The  $\zeta$ -potentials of the ARS-nHAP and the sand grains at varying  $I_c$  conditions and HA = 10 mg L<sup>-1</sup> are shown in Table 1. Both the ARS-nHAP and quartz sand are negatively charged over the tested range of  $I_c$  conditions, consistent with previous results [6,25,30]. The magnitude of the  $\zeta$ -potential diminished with an increase in salt concentration (NaCl) as expected from EDL-compression. These results are also consistent with our previous studies [14,19,21,24].

### 3.2. Sizes of ARS-nHAP

The measured average particle sizes of ARS-nHAP at varying  $I_c$  conditions and HA = 10 mg L<sup>-1</sup> are provided in Table 2. The intensity-weighted hydrodynamic size measured by DLS for ARS-nHAP in the influent was dependent on the suspension  $I_c$ , ranging

**Table 2**

Sizes of ARS-nHAP in the influent and effluent at varying  $I_c$  conditions (pH 7.2 and HA = 10 mg L<sup>-1</sup>).

ARS-nHAP	$I_c$ (mM)	DLS size <sup>a</sup> (nm)	TEM size <sup>b</sup> (nm)
Influent	0.1	250 ± 9.1	101 ± 2.5
	1.0	292 ± 9.2	101 ± 1.6
	10	418 ± 12	101 ± 1.8
	50	638 ± 16	101 ± 1.3
Effluent	0.1	108 ± 8.9	100 ± 1.4
	1.0	196 ± 10	100 ± 1.2
	10	247 ± 13	100 ± 1.4
	50	312 ± 13	100 ± 1.8

<sup>a</sup> The average intensity-weighted hydrodynamic particle size of ARS-nHAP, determined by dynamic light scattering (DLS) measurement.

<sup>b</sup> The average particle size of ARS-nHAP, determined by transmission electron microscopy (TEM) measurement.

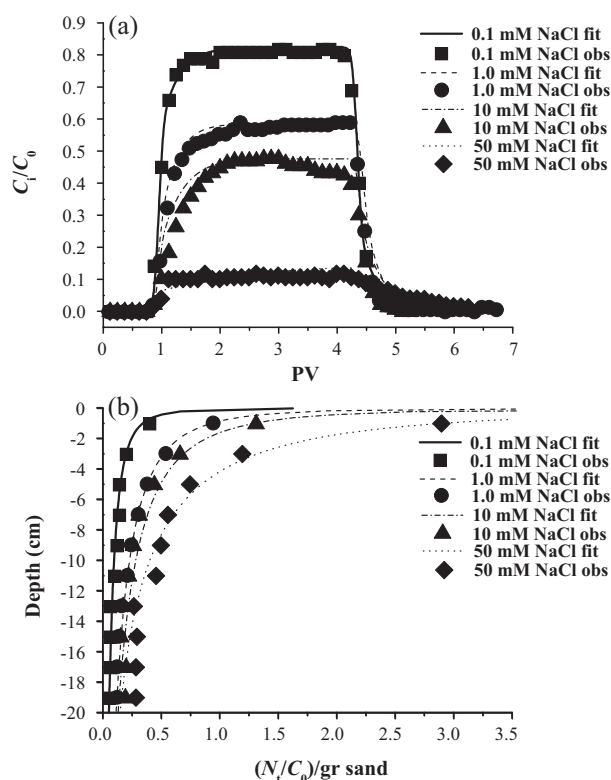


**Fig. 1.** Measured and fitted breakthrough curves (a) and retention profiles (b) for ARS-nHAP at varying  $I_c$  conditions (NaCl as background electrolyte, pH 7.2 and HA = 10 mg L<sup>-1</sup>). Fitted curves were obtained using the two-site kinetic attachment model. In (b) the normalized concentration (quantity of the ARS-nHAP recovered in the sand,  $N_t$ , divided by  $C_0$ ) per gram of dry sand and these are plotted as a function of the distance from the column inlet.

from 250 to 638 nm. The ARS-nHAP size increased substantially with increasing salt concentration, indicating that  $I_c$  decreased the stability of the ARS-nHAP suspension as a result of the decrease in  $\zeta$ -potential (Table 1). Conversely, the average sizes of ARS-nHAP measured by TEM were in the vicinity of 100 nm in length (Table 2). These observations suggest that high  $I_c$  enhanced aggregation. The intensity-weighted hydrodynamic diameter was used in the DLVO calculations because it is more relevant to Brownian transport of the ARS-nHAP than the diameter determined by TEM [30].

### 3.3. Transport of ARS-nHAP at different $I_c$ conditions

Fig. 1a and b present breakthrough curves (BTCs) and retention profiles (RPs), respectively, of ARS-nHAP being advected through quartz sand at different  $I_c$  in the presence of 10 mg L<sup>-1</sup> HA at pH 7.2. The BTCs are plotted as dimensionless concentration  $C_i/C_0$  of ARS-nHAP as a function of PVs. The RPs are plotted as normalized concentration (quantity of the ARS-nHAP recovered in the sand,  $N_t$ , divided by  $C_0$ ) per gram of dry sand as a function of distance from the column inlet. The corresponding mass recovery of ARS-nHAP in the effluent and sand is shown in Table 1, and indicated good mass balance (100–104%). The  $I_c$  was found to have a marked influence on the ARS-nHAP deposition dynamics. Substantial ARS-nHAP retention occurred despite the unfavorable electrochemical conditions for attachments in the primary minimum that are predicted by DLVO theory (Table 1). In general, an increase in  $I_c$  resulted in increasing retention of the ARS-nHAP onto the quartz sand. In particular, the percentage of ARS-nHAP mass that was recovered in the effluent considerably decreased from 78.8 to 7.8% as the  $I_c$  was increased from 0.1 to 50 mM. Greater retention of ARS-nHAP at higher electrolyte concentration can be explained in part by a

**Table 3**

Fitted parameters of the two-site kinetic attachment model as estimated from the breakthrough data for saturated packed column at varying  $I_c$  conditions (pH 7.2 and HA = 10 mg L<sup>-1</sup>).

$I_c$ (mM)	$k_1^a$ (min <sup>-1</sup> )	$k_{1d}^b$ (min <sup>-1</sup> )	$k_2^c$ (min <sup>-1</sup> )	$R^{2d}$
0.1	$1.05 \times 10^{-2}$	$9.96 \times 10^{-2}$	$4.66 \times 10^{-2}$	0.996
1.0	$2.28 \times 10^{-2}$	$1.37 \times 10^{-1}$	$1.35 \times 10^{-1}$	0.984
10	$2.40 \times 10^{-2}$	$1.52 \times 10^{-1}$	$1.76 \times 10^{-1}$	0.965
50	$3.65 \times 10^{-2}$	$2.51 \times 10^{-1}$	$5.12 \times 10^{-1}$	0.993

<sup>a</sup> First-order retention coefficient on site 1.

<sup>b</sup> First-order detachment coefficient on site 1.

<sup>c</sup> First-order retention coefficient on site 2.

<sup>d</sup> Squared Pearson's correction coefficient.

reduction in the thickness of the EDL and corresponding increase in the depth of the secondary minimum (Table 1), consistent with similar studies [6,25,30].

The RPs of ARS-nHAP typically exhibited a hyperexponential shape with greater retention in the section adjacent to the column inlet (0–4 cm) and rapidly decreasing retention rate with transport depth (Fig. 1b). The shape of the RPs was not consistent with colloid filtration theory (CFT) [31] which predicts an exponential shape with depth. Hyperexponential profiles were more pronounced at higher  $I_c$ . Approximately 34.7% of the retained ARS-nHAP occurred near the column inlet when  $I_c = 0.1$  mM, whereas the value was as high as 55.0% in the  $I_c$  of 50 mM (data not shown).

The two-site kinetic retention model provides a good description (squared Pearson's correlation coefficient,  $R^2$ , 0.965–0.996, Table 3) for both the BTCs and RPs. Values of  $k_1$  and  $k_2$  both increased with  $I_c$ , suggesting that the greater retention of ARS-nHAP near the inlet versus the outlet of the column was, in part, related to the depth of the secondary minimum [16,32], and potentially to the surface charge heterogeneities in the ARS-nHAP and the sand grains (discussed in Section 3.4) [15–18]. Fractional retention of ARS-nHAP at type 1 (reversible attachment) and 2 (irreversible attachment) sites were relatively constant with  $I_c$ , ranging from 7 to 18% for type 1 sites and 82 to 93% for type 2 sites. The value of  $k_{1d}$  also increased with  $I_c$  and was even greater than  $k_1$ , consistent with an earlier report [33].

### 3.4. Mechanisms of ARS-nHAP retention

Wang et al. [5] investigated the mechanisms of ARS-nHAP retention for different humic acid concentrations, pHs, and amounts of iron oxyhydroxide coating on sand grains. In brief, retention was demonstrated to depend on ARS-nHAP aggregation, chemical heterogeneity, and on grain surface roughness. In the present study, experiments examining ARS-nHAP retention and causes for hyperexponential RPs will be discussed in order to improve our understanding of the role of chemical heterogeneity.

A shallow secondary minimum (ca.  $-0.075$  to  $-1.7 K_B T$  (see Table 1), where  $K_B$  is the Boltzmann constant,  $T$  is the absolute temperature) occurred in the experiments where  $I_c$  was varied, resulting in decreasing transport and increasing ARS-nHAP retention with increasing  $I_c$  (Fig. 1a). This suggests that NP retention was influenced to a substantive degree within the secondary minimum. However, Fig. 2 indicates that only a negligible (0–0.4% for  $I_c$  of 50 and 0.1 mM, respectively) amount of ARS-nHAP was recovered during phase 3 when the secondary minimum was eliminated in the presence of DI ( $I_c \leq 10^{-5}$  M) water [34]. The latter observations suggest that, although the secondary minimum was likely involved in the ARS-nHAP retention, it did not account for all of the retained mass of ARS-nHAP.

Given the low degree of ARS-nHAP recovery in the presence of DI water, other factors were likely contributing to ARS-nHAP retention and release. For example, flow interruption

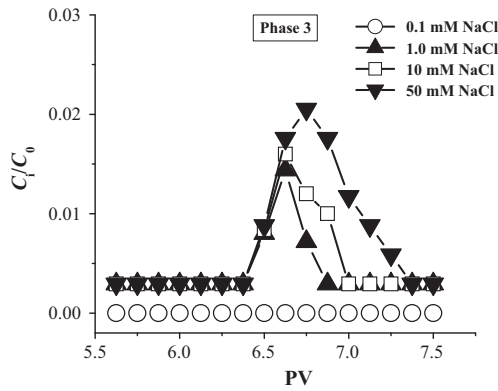


**Fig. 2.** Representative breakthrough curves for ARS-nHAP in the presence of varied background electrolyte (NaCl) concentrations of 0.1, 1.0, 10, and 50 mM (pH 7.2 and HA = 10 mg L<sup>-1</sup>). Phase 3 consisted of flushing several pore volumes of DI ( $I_c < 10^{-5}$  M) water to eliminate the secondary minimum.

at the end of the experiment released only a trace amount of ARS-nHAP, which likely represented the quantity of NPs associated with stagnant parcels of water within the pore structure [35]. In contrast, data in Table 1 indicate that much of the retained ARS-nHAP could be recovered by destroying the pore structure, suggesting that the retained ARS-nHAP was likely in an aggregated form. The ARS-nHAP particle size tended to increase with increasing  $I_c$  of bulk suspension for both influent and effluent. The average NP size increased more than two-fold (from 250 to 638 nm) and about three-fold (from 108 to 312 nm) for influent and effluent respectively, when the background electrolyte (NaCl) concentration was increased from 0.1 to 50 mM (Table 2). This observation further confirms that the ARS-nHAP was likely retained in an aggregated form. Sizes of ARS-nHAP in the effluent also increased with increasing  $I_c$ , but always to a lesser degree than those in the influent. This was due to the size-selective effect of the granular media, consistent with our previous study [5].

Hyperexponential RPs occurred during all of the considered  $I_c$  conditions. Surface charge heterogeneity in the colloid population has been reported to play an important role in creating hyperexponential RPs under unfavorable attachment condition [15–18]. In order to test this hypothesis, the  $\zeta$ -potentials of ARS-nHAP at varying  $I_c$  conditions were measured before and after filtering them through a 1  $\mu$ m pore diameter glass fiber filter. As shown in Fig. 3a, the  $\zeta$ -potentials of ARS-nHAP became progressively more negative after filtering. Li et al. [15] reported that such a variation in the  $\zeta$ -potential was sufficient to cause hyperexponential RPs. That is, the fraction of the ARS-nHAP population with higher  $\zeta$ -potentials (less negative) is assumed to preferentially attach at the column inlet, whereas the remaining NPs experience a slower attachment rate and greater transport potential. Here, we introduce  $\Delta\zeta$  (%) to evaluate the degree of the  $\zeta$ -potential variation before and after filtering at varying  $I_c$  as:

$$\left\{ \Delta\zeta(\%) = \frac{\zeta_{\text{after}} - \zeta_{\text{before}}}{\zeta_{\text{before}}} \times 100\% \right\} \quad (5)$$

where  $\zeta_{\text{before}}$  (mV) and  $\zeta_{\text{after}}$  (mV) are the  $\zeta$ -potentials of ARS-nHAP before and after filtering them through a 1  $\mu$ m pore diameter glass fiber filter, respectively. As shown in Fig. 3b, the value of the  $\Delta\zeta$  substantially increased from 3.4 to 4.9, 14, and 26% when the  $I_c$  was increased, respectively, from 0.1 to 1.0, 10, and 50 mM, respectively. Hence, greater variations existed within the population of ARS-nHAP at higher  $I_c$ . It is reasonable to assume that at higher  $I_c$ , larger portions of ARS-nHAP are likely to attach preferentially at the column inlet because of an increase in  $\Delta\zeta$ , aggregate size (Table 2),

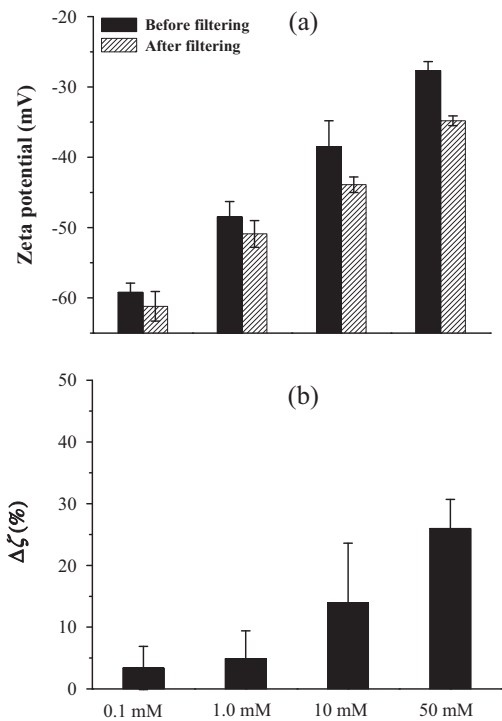


**Fig. 3.**  $\zeta$ -potentials of ARS-nHAP suspensions before and after filtering them through a 1  $\mu$ m pore diameter glass fiber filter (a) and the degree ( $\Delta\zeta$ ) of the  $\zeta$ -potential variation (b) at varying  $I_c$  conditions (pH 7.2 and HA = 10 mg L<sup>-1</sup>). Error bars represent standard deviations.

and depth of the secondary minimum (Table 1). This, in turn, causes more pronounced hyperexponential deposition behaviors.

Surface charge heterogeneity in the collector surfaces has also been reported to contribute to the hyperexponential RPs under unfavorable attachment conditions [16]. In order to test this hypothesis, we ran another two phase experiment using 100 mg L<sup>-1</sup> ARS-nHAP at  $I_c$  of 50 mM, pH of 7.2, and HA concentration of 10 mg L<sup>-1</sup>. Prior to the injection of ARS-nHAP, the column was pre-equilibrated with 10 PVs of 10 mg L<sup>-1</sup> HA solution at 50 mM  $I_c$ , followed by introduction of 5 PVs of background electrolyte solution (also  $I_c = 50$  mM) in order to assess the effect of pretreating the granular media with HA on the transport of ARS-nHAP. In comparing ARS-nHAP BTC for the untreated and HA-treated sands (Fig. 4), it is evident that the dimensionless concentrations in the “steady-state” portion of the NP BTC was subject to considerably less variability in the HA-treated system. This observation indicates that there is considerable spatial variability in surface charge on the

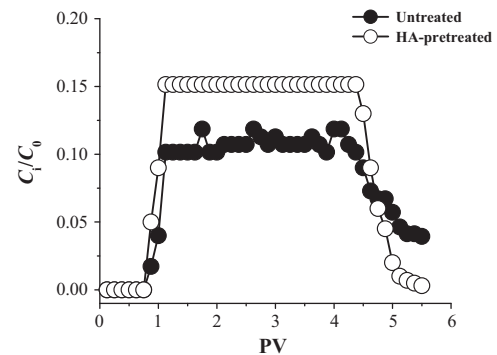


**Fig. 4.** Representative breakthrough curves for ARS-nHAP as a function of pore volumes (PVs) in untreated and 10 mg L<sup>-1</sup> HA-pretreated quartz sand columns at  $I_c$  of 50 mM NaCl (pH 7.2).

collector surfaces and that HA may even this out. These results are consistent with those reported earlier [16,36].

In addition, the ARS-nHAP mass recovery ( $M_{\text{eff}}$ ) was up to 12.2% in HA pretreated sand ( $M_{\text{eff}} = 7.8\%$  in untreated sand). Some authors have attributed the greater transport of NPs through sand pretreated with HA to enhanced electrostatic repulsion between colloid and collector surface which results from negatively charged carboxylate and phenolate functional groups on the sorbed HA [36]. In order to confirm this hypothesis, we measured streaming potentials of the sand grain in the absence and presence of HA ( $10 \text{ mg L}^{-1}$ ) and found that the  $\zeta$ -potentials increased in magnitude from  $-21.4$  to  $-25.7$  mV when the equilibration suspension HA concentration increased from 0 to  $10 \text{ mg L}^{-1}$ . This observation confirms that HA acts to modify the surface charge of the collector by imparting more negative charge and (or) by masking some of the positive charge associated with impurities (iron or aluminum oxyhydroxides) [16], which reduces ARS-nHAP deposition.

#### 4. Conclusions

Packed column experiments were conducted to investigate the transport and retention of ARS-nHAP at varying  $I_c$  and  $\text{HA} = 10 \text{ mg L}^{-1}$ . The transport of ARS-nHAP strongly depended upon  $I_c$ . Total mass recovery for ARS-nHAP decreased ten-fold from 78.8% to 7.8%, when background electrolyte concentration increased from 0.1 to 50 mM NaCl with a corresponding compression of the ARS-nHAP EDL. Most of the ARS-nHAP was retained close to the column inlet (0–4 cm). The deposition profile within the column was hyperexponential with the rate of retention rapidly decreasing with travel distance. The experimental BTCs and RPs of ARS-nHAP were well described using a two-site kinetic attachment model. The first-order attachment coefficients associated with sites 1 and 2, i.e.,  $k_1$  and  $k_2$ , respectively, both increased with  $I_c$ . This was due in part to a calculated increase in the depth of the secondary minimum, the aggregate size, and  $\Delta\zeta$ . The RPs were hyperexponential for the range of electrolyte concentrations considered. Surface charge heterogeneities among the ARS-nHAP population and in the grain surface appeared to be the primary cause of the hyperexponential RPs observed in the present study.

Given the complexities and heterogeneities that characterize contaminated soils and aquifers, it is important to understand how variations in environmentally relevant concentrations of dissolved salts and dissolved organic matter (DOM) can affect the transport behavior of NPs introduced to the subsurface for the purposes of remediation. Because the number and range of salient variables in the aquifer cannot be replicated easily in column studies, field studies in the form of controlled injection-and-recovery experiments would result in additional information relating to the transport behavior nHAP in natural granular media. Judging from the column results described herein, use of the temporally stable and easily discernible fluorescent ARS label should facilitate tracking of nHAP in the natural environment. The caveat is that ARS-labeled nHAP proved to be more negatively charged than unlabeled nHAP, because of hydroxyl and carbonyl functions groups on the ARS. Consequently, differences in transport potential between ARS-tagged and untagged nHAP would need to be taken into account when using ARS-nHAP in the field. The column studies further indicate that the transport of nHAP is very sensitive to the presence of even minute (e.g.,  $10 \text{ mg L}^{-1}$ ) concentrations of HA, as evidence by consequential decreases in the NP zeta potential and fractional breakthrough within the columns. Because metal- and radionuclide-contaminated aquifers can be characterized by more reactive (and more abundant) natural and contaminant dissolved organic carbon, the role of DOC on the transport of nHAP in the field will need to be considered and is a topic worthy of further study.

#### Acknowledgments

This work was supported by the Knowledge Innovative Project of Chinese Academy of Sciences (KZCX2-YW-Q02-02) and the National Basic Research and Development Program (2007CB936604). Any use of trade, firm, or product names is for description purposes only and does not imply endorsement by the U.S. Government.

#### Appendix A. Supplementary data

Supplementary data associated with this article can be found, in the online version, at <http://dx.doi.org/10.1016/j.jhazmat.2012.05.089>.

#### References

- [1] S. Handley-Sidhu, J.C. Renshaw, S. Moriyama, B. Stolpe, C. Mennan, S. Bagheriasl, P. Yong, A. Stamboulis, M. Paterson-Beedle, K. Sasaki, R.A.D. Patrick, J.R. Lead, L.E. Macaskie, Uptake of  $\text{Sr}^{2+}$  and  $\text{Co}^{2+}$  into biogenic hydroxyapatite: implications for biomineral ion exchange synthesis, *Environ. Sci. Technol.* 45 (2011) 6985–6990.
- [2] Q.Y. Ma, S.J. Traina, T.J. Logan, J.A. Ryan, Effects of aqueous Al, Cd, Cu, Fe(II), Ni, and Zn on Pb immobilization by hydroxyapatite, *Environ. Sci. Technol.* 28 (1994) 1219–1228.
- [3] E.H. Oelkers, J.M. Montel, Phosphates and nuclear waste storage, *Elements* 4 (2008) 113–116.
- [4] Y.J. Wang, J.H. Chen, Y.X. Cui, S.Q. Wang, D.M. Zhou, Effects of low-molecular-weight organic acids on Cu(II) adsorption onto hydroxyapatite nanoparticles, *J. Hazard. Mater.* 162 (2009) 1135–1140.
- [5] D.J. Wang, S.A. Bradford, R.W. Harvey, B. Gao, L. Cang, D.M. Zhou, Humic acid facilitates the transport of ARS-labeled hydroxyapatite nanoparticles in iron oxyhydroxide-coated sand, *Environ. Sci. Technol.* 46 (2012) 2738–2745.
- [6] N. Saleh, H.J. Kim, T. Phenrat, K. Matyjaszewski, R.D. Tilton, G.V. Lowry, Ionic strength and composition affect the mobility of surface-modified  $\text{Fe}^0$  nanoparticles in water-saturated sand columns, *Environ. Sci. Technol.* 42 (2008) 3349–3355.
- [7] B. Derjaguin, L. Landau, Theory of the stability of strongly charged lyophobic sols and the adhesion of strongly charged particles in solutions of electrolyte, *Acta Physicochim. URSS* 14 (1941) 733–762.
- [8] E.J.W. Verwey, J.T.G. Overbeek, Theory of the Stability of Lyophobic Colloids, Elsevier, Amsterdam, The Netherlands, 1948.
- [9] R.D. Duffadar, J.M. Davis, Interaction of micrometer-scale particles with nanotextured surfaces in shear flow, *J. Colloid Interface Sci.* 308 (2007) 20–29.
- [10] R.D. Duffadar, J.M. Davis, Dynamic adhesion behavior of micrometer-scale particles flowing over patchy surfaces with nanoscale electrostatic heterogeneity, *J. Colloid Interface Sci.* 326 (2008) 18–27.
- [11] K.L. Chen, M. Elimelech, Interaction of fullerene (C60) nanoparticles with humic acid and alginate coated silica surfaces: measurements, mechanisms, and environmental implications, *Environ. Sci. Technol.* 42 (2008) 7607–7614.
- [12] H. Hyung, J.D. Fortner, J.B. Hughes, J.H. Kim, Natural organic matter stabilizes carbon nanotubes in the aqueous phase, *Environ. Sci. Technol.* 41 (2007) 179–184.
- [13] B. Xie, Z.H. Xu, W.H. Guo, Q.L. Li, Impact of natural organic matter on the physicochemical properties of aqueous  $\text{C}_{60}$  nanoparticles, *Environ. Sci. Technol.* 42 (2008) 2853–2859.
- [14] L.Y. Chu, D.J. Wang, Y.J. Wang, Y.B. Si, D.M. Zhou, Transport of hydroxyapatite nanoparticles in saturated packed column: effects of humic acid, pH and ionic strengths, *Environ. Sci.* 32 (2011) 2284–2291 (in Chinese).
- [15] X.Q. Li, T.D. Scheibe, W.P. Johnson, Apparent decreases in colloid deposition rate coefficients with distance of transport under unfavorable deposition conditions: a general phenomenon, *Environ. Sci. Technol.* 38 (2004) 5616–5625.
- [16] N. Tufenkji, M. Elimelech, Breakdown of colloid filtration theory: role of the secondary energy minimum and surface charge heterogeneities, *Langmuir* 21 (2005) 841–852.
- [17] Y.S. Li, Y.G. Wang, K.D. Pennell, L.M. Abriola, Investigation of the transport and deposition of fullerene (C60) nanoparticles in quartz sands under varying flow conditions, *Environ. Sci. Technol.* 42 (2008) 7174–7180.
- [18] S. Torkzaban, Y. Kim, M. Mulvihill, J.M. Wan, T.K. Tokunaga, Transport and deposition of functionalized CdTe nanoparticles in saturated porous media, *J. Contam. Hydrol.* 118 (2010) 208–217.
- [19] D.J. Wang, L.Y. Chu, M. Paradelo, W.J.G.M. Peijnenburg, Y.J. Wang, D.M. Zhou, Transport behavior of humic acid-modified nano-hydroxyapatite in saturated packed column: effects of Cu, ionic strength, and ionic composition, *J. Colloid Interface Sci.* 360 (2011) 398–407.
- [20] M. Vukomanovic, T. Zavanik-Bergant, I. Bracko, S.D. Skapin, N. Ignjatovic, V. Radmilovic, D. Uskokovic, Poly(D,L-lactide-co-glycolide)/hydroxyapatite core-shell nanospheres. Part 3: properties of hydroxyapatite nano-rods and investigation of a distribution of the drug within the composite, *Colloids Surf. B* 87 (2011) 226–235.

- [21] D.M. Zhou, D.J. Wang, L. Cang, X.Z. Hao, L.Y. Chu, Transport and re-entrainment of soil colloids in saturated packed column: effects of pH and ionic strength, *J. Soils Sediments* 11 (2011) 491–503.
- [22] T. Moriguchi, K. Yano, S. Nakagawa, E. Kaji, Elucidation of adsorption mechanism of bone-staining agent Alizarin red S on hydroxyapatite by FT-IR microspectroscopy, *J. Colloid Interface Sci.* 260 (2003) 19–25.
- [23] D.J. Wang, S.A. Bradford, M. Paradelo, W.J.G.M. Peijnenburg, D.M. Zhou, Facilitated transport of copper with hydroxyapatite nanoparticles in saturated sand, *Soil Sci. Soc. Am. J.* 76 (2012) 375–388.
- [24] D.J. Wang, M. Paradelo, S.A. Bradford, W.J.G.M. Peijnenburg, L.Y. Chu, D.M. Zhou, Facilitated transport of Cu with hydroxyapatite nanoparticles in saturated sand: effects of solution ionic strength and composition, *Water Res.* 45 (2011) 5905–5915.
- [25] M. Elimelech, J. Gregory, X. Jia, R.A. Williams, *Particle Deposition and Aggregation: Measurement Modeling and Simulation*, Butterworth-Heinemann, Oxford, U.K, 1995.
- [26] S.A. Bradford, J. Simunek, M. Bettahar, M.T. van Genuchten, S.R. Yates, Modeling colloid attachment, straining, and exclusion in saturated porous media, *Environ. Sci. Technol.* 37 (2003) 2242–2250.
- [27] J.F. Schijven, J. Simunek, Kinetic modeling of virus transport at the field scale, *J. Contam. Hydrol.* 55 (2002) 113–135.
- [28] J. Simunek, M.T. van Genuchten, M. Sejna, The HYDRUS-1D software package for simulating the one-dimensional movement of water, heat, and multiple solutes in variably saturated media, in: Version 4.0, HYDRUS Software Series 3, Department of Environmental Science, University of California Riverside, Riverside, California, 2008.
- [29] D.W. Marquardt, An algorithm for least-squares estimation of nonlinear parameters, *J. Soc. Ind. Appl. Math.* 11 (1963) 431–441.
- [30] G.X. Chen, X.Y. Liu, C.M. Su, Transport and retention of TiO<sub>2</sub> rutile nanoparticles in saturated porous media under low-ionic-strength conditions: measurements and mechanisms, *Langmuir* 27 (2011) 5393–5402.
- [31] K.M. Yao, M.M. Habibian, C.R. O'Melia, Water and waste water filtration: concepts and applications, *Environ. Sci. Technol.* 5 (1971) 1105–1112.
- [32] S.A. Bradford, S. Torkzaban, F. Leij, J. Simunek, M.T. van Genuchten, Modeling the coupled effects of pore space geometry and velocity on colloid transport and retention, *Water Resour. Res.* 45 (2009), <http://dx.doi.org/10.1029/2008WR007096>.
- [33] G. Gargiulo, S.A. Bradford, J. Simunek, P. Ustohal, H. Vereecken, E. Klumpp, Transport and deposition of metabolically active and stationary phase *Deinococcus radiodurans* in unsaturated porous media, *Environ. Sci. Technol.* 41 (2007) 1265–1271.
- [34] A. Franchi, C.R. O'Melia, Effects of natural organic matter and solution chemistry on the deposition and reentrainment of colloids in porous media, *Environ. Sci. Technol.* 37 (2003) 1122–1129.
- [35] S. Torkzaban, H.N. Kim, J. Simunek, S.A. Bradford, Hysteresis of colloid retention and release in saturated porous media during transients in solution chemistry, *Environ. Sci. Technol.* 44 (2010) 1662–1669.
- [36] H.Y. Yang, H. Kim, M.P. Tong, Influence of humic acid on the transport behavior of bacteria in quartz sand, *Colloids Surf. B* 91 (2012) 122–129.